Heliyon 7 (2021) e05993

Contents lists available at ScienceDirect

Heliyon

journal homepage: www.cell.com/heliyon

Research article

Sustainable removal of anodized aluminum dye by groundwater treatment waste: experimental and modeling

Edita Sodaitienė, Audronė Gefenienė *, Danutė Kaušpėdienė, Romas Ragauskas, Jūratė Vaičiūnienė, Aušra Selskienė, Vitalija Jasulaitienė, Rimantas Ramanauskas

Center for Physical Sciences and Technologies, Saulėtekio av. 3, Vilnius 10257, Lithuania

ARTICLE INFO

Keywords:
Adsorption
Groundwater treatment waste
Anodized aluminum dye
Kinetics
Equilibrium
Thermodynamics

ABSTRACT

Groundwater treatment waste (GWTW), as an environmentally friendly renewable nanomaterial, was implemented for the removal of anodized aluminum dye Sanodure Green (SG) from aqueous solutions. The capability of the SG metal complex dye removal was assessed by measuring solution decoloration and chromium elimination degree. GWTW was characterized using FTIR, SEM, EDX, TEM, XPS and surface area measurements. Kinetic curves were obtained by changing initial dye concentration, pH, temperature and adsorbent dose. Kinetic studies showed that up to 90 % of SG dye was removed within a contact time of 20 min. The adsorption of the dye was favourable at 293 K temperature in the acidic pH region (pH 1.5–2.0) with maximum adsorption capacity 185 mg g^{-1}. Langmuir-Freundlich isotherm model as well as hyperbolic tangent, diffusion-chemisorption and Elovich kinetic models accurately describe the dye removal process. The calculated thermodynamic parameters confirmed that SG dye removal occurred spontaneously and exothermically. The magnitude of enthalpy change ($\Delta H^{\circ} = -35.80$ kJ mol^{-1}) was in agreement with the electrostatic interaction. The adsorption potential of GWTW for SG dye removal was also evaluated using a real wastewater produced after dyeing of anodized aluminum.

1. Introduction

Dyeing processes can be classified as environmentally harmful processes (Wang and Li, 2007). Different types of physical, chemical, electrochemical and biological methods are used for decolorization of industrial wastewater (Collivignarelli et al., 2019). Coagulation-flocculation, membrane treatment, advanced oxidation process, biological degradation, adsorption and various other technologies are frequently applied to discard dyes from water (Grace Pavithra et al., 2019; Collivignarelli et al., 2019; Nourmoradi et al., 2015).

Nanostructured metal oxides, their composites (Gusain et al., 2019) and hybrids of the layered double hydroxide (Daud et al., 2019) have shown excellent adsorption performance in the removal of toxic organic dyes from wastewater. Among them, the iron oxide nanomaterials in the pure, doped, and composite forms have been extensively used for adsorption of the organic pollutants (Vu and Vu, 2018). Magnetic iron oxide nanospheres consisting of both Fe_3O_4 and α-Fe_2O_3 were prepared for removal of Reactive Orange (RO) and Reactive Yellow (RY) anionic dyes from model aqueous solutions (Khosravi and Azizian, 2014a). Flower-like iron oxides with different nanostructure were synthesized with the ability to remove dyes from water within few minutes (Khosravi and Azizian, 2014b). The microporous-mesoporous FeMgO adsorbents were produced by impregnation, co-precipitation and hydrothermal methods. Powdered $Mg(OH)_2$ was impregnated with aqueous iron nitrate solution and the resulted paste was dried and calcined. Using co-precipitation method, iron and magnesium nitrates were co-precipitated from mixture solution with NH_3, dried and calcined. Hydrothermal method includes heating the suspension of iron and magnesium hydroxides in autoclave. Water from the obtained colloidal solution was removed by heating at 50 °C. FeMgO adsorbents were tested in the removal of Remazol Red RB-133 textile dye from synthetic solutions (Mahmoud et al., 2013). Phthalocyanine based commercial dye C. I. Reactive Blue 21 was selected for batch decolorization studies using Fe–Ni nanoparticles (Kale and Kane, 2019).

Efficient low-cost adsorbents can be prepared by reusing different types of waste. An example of this novel approach could be the synthesis of Fe_2O_3 microspheres from natural ilmenite followed by application for the adsorption of three organic dyes, specifically for Congo red, Methyl orange and Methylene blue (Kang et al., 2018).

The preparation of drinking water from surface and groundwater generates large amounts of solid waste, named as water treatment residuals (WTRs) (Deliz Quiñones et al., 2016; Castaldi et al., 2014;

* Corresponding author.
E-mail address: audrone.gefeniene@ftmc.lt (A. Gefenienė).

https://doi.org/10.1016/j.heliyon.2021.e05993
Received 13 August 2020; Received in revised form 26 November 2020; Accepted 12 January 2021

Novoselova, 2013; Ociński et al., 2016). Due to the appropriate physicochemical properties, this waste is being tested for the treatment of water contaminated with dyes. WTRs produced after the use of polyaluminum chloride (PACl) for the preparation of drinking water, were applicated in the studies of color removal of Disperse Blue 79 dye from synthetic wastewater (Gadekar and Ahammed, 2018). The experimental color removal efficiency of 52 % was close to that predicted by the theoretical models. Color removal performance using recycled alum sludge was also examined by Chu (2001). Two commercial dyes, an anionic disperse dye Dianix Blue FBL-E and an anionic direct dye Ciba-corn Yellow P-6GS, were selected for the study. Not only aluminum based, but also iron based waterworks sludge could be considered as alternative adsorbent for the effective and cheap treatment of colored textile wastewater. The applicability of this waste for the adsorption of cationic (Basic Violet 16), anionic (Direct Blue 71, Acid Blue 40, and Reactive Blue 29) and non-ionic (Disperse Brown 19) dyes was tested (Kayranli, 2011). In addition, solid waste generated during drinking water treatment can be applied as coagulants. Acid Red 119 dye removal by coagulation-floculation using two different types of waterworks sludge, ferric chloride sludge (FCS) and polyaluminum chloride sludge (PACS), was studied. The performance of ferric chloride sludge was more outstanding than that of PACS in the removal of AR119 dye (Moghaddam et al., 2010).

Groundwater treatment sludge was converted to magnetic particles to make it more convenient to use in adsorption system. The efficiency of the prepared adsorbents was examined using methylene blue dye solutions (Zhu et al., 2015). The removal of Navy blue textile dye by two step process was investigated by Nourmoradi et al. Ferric chloride and some other coagulants were used in the first step of the dye solution treatment. In the second step, clay minerals, montmorillonite and nano-montmorillonite, were suitable for the removal of residual color by adsorption (Nourmoradi et al., 2015). Activated carbon derived from coconut shells was used as the adsorbent and aluminum chloride was used as the coagulant for the removal of reactive dyes Black 5 and Orange 16 (Furlan et al., 2010). Kim et al. (2004) studied the processes of destabilization and decoloration of commercial dye solutions using ferric chloride. The authors came to the conclusion that disperse dyes can be removed more effectively when compared to reactive dyes.

Metal complex dyes are widely used for the coloring of wood, leather, plastic and metals (Mahapatra, 2016). At the open access facility of the Center of Physical Sciences and Technology in Vilnius (Lithuania) a small scale manufacturing of specialized products is carried out. The colored anodized aluminum parts are fabricated for information technology equipment, lasers, robots, etc. Sanodure Green LWN (SG) metal complex dye is a representative dye used for adsorptive coloration of anodized aluminum (http://waynehilldesign.com/images/brochures/RAP_capabilities.pdf). The dye deposited on the surface of aluminum oxide provides the transparent layer that reflects the colour (Chang et al., 2016). Chemically SG dye can be characterized as chromium complex organic dye, therefore should not be allowed to enter drains, water sources or the soil (Sanodure Green LWN safety data sheet, 2020). The wastewater produced after dying and rinsing of aluminum parts should be decolorized and heavy metal ions extracted out of solution. The need for environmental sustainability supports an idea to utilize for the treatment of wastewater a local waste generated spontaneously during the aeration and filtration of groundwater. The solid groundwater treatment waste (GWTW) with the main component of ferric oxide/hydroxide represents a natural nanomaterial with the properties similar to artificially synthesized adsorbents. A number of studies have shown that waste from drinking water treatment processes has a relatively large surface area and can therefore be used as adsorbent. The BET method revealed the surface area of Al-based WTRs averaging 48 $m^2\ g^{-1}$ (Deliz Quiñones et al., 2016), whereas, the commercial α-Fe_2O_3 powders have a much lower BET area of 18 $m^2\ g^{-1}$ (Su et al., 2012). A specific surface area S_{BET} of the Fe-based WTRs obtained using $Fe_2(SO_4)_3$ as the coagulant was equal to 35 $m^2\ g^{-1}$ (Castaldi et al., 2014). The specific surface area of fresh GWTW produced during cascade aeration of infiltration water was 120 $m^2\ g^{-1}$ (Ociński et al., 2016).

The aim of our study was to determine the suitability and reusability of GWTW for SG dye removal from model aqueous solutions and to ascertain the chemical behavior of the adsorption system by changing the process conditions. The dye removal efficiency was evaluated considering not only solution decoloration but also chromium retention degree. This is relevant because a small proportion of chromium ions present in the composition of metal complex dye remains uncomplexed. The impact of the process conditions on its efficiency was studied varying adsorbent and adsorbate concentration, their contact time, solution pH and adsorption system temperature. The adsorptive properties of GWTW were assessed through kinetic, equilibrium and thermodynamic investigations. GWTW adsorbent was also applied for the treatment of real wastewater obtained after dyeing of anodized aluminum.

2. Experimental

2.1. Preparation of Sanodure Green (SG) dye solutions

Sanodure Green LWN (SG) dye (Clariant) is water-soluble anionic chromium complex azo dye widely applied in anodized aluminum dyeing process. It was commercial grade and was used without further purification. The dye stock solution was made by mixing 1000 mg of SG dye in 1 L of deionized water. Then it was diluted with deionized water to obtain solutions of the desired concentration. The pH was adjusted by 5 M HCl or 0.1 M and 1 M NaOH. The values of pH were measured using inoLab 7110 pH meter (WTW-Germany). All chemical reagents used were Analytical Reagent Grade.

2.2. Groundwater treatment waste

The iron-based groundwater treatment waste was obtained from drinking water treatment plant in Vilnius, Lithuania. The GWTW is produced as a result of the deironing and demanganization of groundwater by cascade aeration. The collected waste was stored at room temperature (20–25 °C) in its original form and was used in its raw state after grinding in a mortar. The brown powder is mostly composed of iron oxide/hydroxide (Zubrytė et al., 2019). The morphology of GWTW surface and chemical composition of the GWTW was studied by SEM-EDX and TEM. SEM-EDX analysis was performed on the samples using a scanning electron microscope Helios Nanolab 650 (FEI) equipped with an energy dispersive X-ray spectrometer (Oxford Instruments, Xmax 20 mm^2 detector, INCA 4.15 software). The operating conditions for particles morphology investigation were as follows: secondary electron imaging (SEI), acceleration voltage 2 kV, beam current 0.8 nA. The operating conditions for elemental composition analysis were: acceleration voltage 20 kV, beam current 3.2 nA. Transmission electron microscope (TEM) Tecnai G2 F20 X-TWIN (FEI, Netherlands, 2011) with Schottky type field emission electron source was used to obtain TEM images of GWTW. Prior to scanning, the samples were coated with a conductive film of carbon in a vacuum equipment Quorum Q 150 ES (Quorum). The zeta potential of GWTW was measured using Zetasizer Nano ZS (Malvern Panalytical).

For comparative study of SG dye adsorption capacity five commercially available adsorbents were used including activated carbon NORIT PK 1–3 (Cabot Norit), weak base macroporous resin Macronet MN 150 (Purolite Company), non-ionic macroporous resin Macronet MN 200 (Purolite Company), macroporous strong acid resin Macronet MN 500 (Purolite Company) and mixed bed resin PMB 101 (Pure Resin Co., Ltd).

2.3. Analysis of solutions

The concentration of chromium, calcium and iron in aqueous solutions were determined with an ICP optical emission spectrometer (Optima 7000DV from Perkin Elmer) at 267.716, 317.933 and 238.204 nm, respectively. The concentration of the SG dye solutions was analysed

using Varian Cary 50 UV-Vis spectrophotometer from Agilent Technologies at a wavelength of 630 nm and calculated from a calibration curve. A linear relationship between the concentration of SG dye and the content of chromium in the composition of the dye is presented in Figure 1S.

2.4. BET analysis

The surface area, pore size and pore volume of GWTW were estimated by N_2 adsorption/desorption isotherms collected at 77 K using Brunauer Emmet Teller (BET) method. Pore size distribution (PSD) plot was calculated by the Barrett–Joyner–Halenda (BJH) method using the desorption branch in a Micromeritics Tri-Star II 3020 nitrogen adsorption apparatus.

2.5. FTIR analysis

Identification of functional groups on GWTW was carried out using Fourier Transform Infrared Spectrometer ALPHA (Bruker, Germany), equipped with a room temperature detector DLATGS. Samples were dispersed in KBr tablets. Spectra were acquired from 100 scans in the spectral range of 650–4000 cm^{-1}.

2.6. XPS analysis

Surface composition of GWTW samples and chemical states of elements were investigated by XPS measurements. Vacuum Generator (VG) ESCALAB MKII spectrometer fitted with a XR4 twin anode was used for XPS analysis. MgK_α X-ray was as the X-ray source. The measurements were proceeded at $h\nu = 1253.6$ eV with 300 W power (20mA/15kV). During spectral acquisition the pressure in the analysis chamber was lower than 5×10^{-7} Pa. The survey spectra were obtained using an electron analyser pass energy of 100 eV, the narrow scans – with 20 eV and resolution of 0.05 eV. All spectra were recorded at a 90° take-off angle. Binding energy (BE) referencing was done using the C1s peak at 284.8 eV. Avantage software (v5.962) provided by Thermo VG Scientific was used for the spectra calibration, processing and fitting. Core-level spectra of C1s were fitted with a 70 % Gaussian–30% Lorentzian function and a Shirley background was applied to all spectra.

2.7. Kinetic studies

Behavior of SG dye adsorption by GWTW was investigated using batch technique. In the kinetic experiments, 0.2–0.35 g of GWTW powder was added into conical flasks containing 50 mL of SG dye solutions with the adjusted pH values. The magnetic stirrer was used operating at 500 rpm. The samples were taken at 0, 3, 5, 10, 20, 40, 60, 120 and 180 min. The experiments were repeated three times. Experimental design for the investigation of various effects on SG dye adsorption kinetics is presented in Table 1S.

The amount of dye taken up and the percentage of the dye removed by the GWTW were calculated by applying Eqs. (1) and (2), respectively:

$$q_t = \frac{(C_0 - C_t)}{m} \cdot V \tag{1}$$

$$\mathrm{RE} = \frac{(C_0 - C_t)}{C_0} \cdot 100\% \tag{2}$$

where q_t (mg g^{-1}) is the mass of SG dye adsorbed per unit mass of GWTW at time t; C_o (mg L^{-1}) is initial concentration of SG dye, C_t (mg L^{-1}) is concentration of SG dye at time t; m (g) is the mass of GWTW, V (L) is the volume of solution, and RE is removal efficiency.

2.7.1. Effect of initial SG dye concentration

Kinetic curves were obtained at room temperature by using SG dye solutions with pH 2 and the initial concentrations 168, 345, 495 and 635 mg L^{-1}.

2.7.2. Effect of SG dye solution pH

To study the effect of SG dye solution pH on adsorption behavior of GWTW, the initial pH was adjusted to different pH values by adding 5 M HCl. Experiments were carried out with initial SG dye concentration of 150 mg L^{-1} at 20 °C temperature, pH_0 1.5–4 without the correction of pH value of adsorption system during adsorption process.

2.7.3. Effect of temperature

Investigation of the action of temperature on the adsorption of SG dye by GWTW was performed at 20 ± 1, 40 ± 1 and 60 ± 1 °C. Flasks containing 0.25 g of GWTW and 50 mL of the 150 mg L^{-1} SG dye solution with pH 2 were shaken for 180 min. The experiments were replicated thrice.

2.7.4. Effect of GWTW dosage

Effect of the adsorbent dose was investigated using the initial SG dye solution concentration of 150 mg L^{-1}. GWTW dose was from 0.20 to 0.35 g at fixed pH value 2 and temperature of 20 °C.

2.8. Equilibrium adsorption

The equilibrium adsorption studies for evaluation of the ability of GWTW to remove SG dye from aqueous solutions were carried out in triplicate, and the error bars represent standard deviation. For these experiments, 0.25 g of GWTW was placed in 50 mL conical flasks containing 50.0 mL of dye solution (50.00–1000.0 mg L^{-1}), which were agitated for 8 h at three different temperatures (293, 313 and 323 K). The pH of the dye solutions was 2, regulated with 5 M HCl. After equilibrium, in order to separate the GWTW from the aqueous solutions, 10 mL of samples were filtered. Remaining concentration of the SG dye and chromium in the solution were determined by the methods mentioned in "Analysis of solutions".

2.9. SG dye desorption study

Regeneration of SG dye saturated adsorbent GWTW was performed by using 0.05 M NaOH solution. The GWTW was weighed before and after desorption. In desorption experiments the ratio of saturated adsorbent and NaOH solution was 1:40. Then the GWTW was washed with deionized water to pH 7 and dried at 60 °C in the furnace. Desorption capacity (mg g^{-1}) and efficiency (%) were calculated using the following equations (Momina et al., 2020):

$$q_{e,\,desorp} = V\left(\frac{C_f}{M}\right) \tag{3}$$

$$Q = \frac{q_{e,\,desorp}}{q_{e,sorp}} \cdot 100 \tag{4}$$

where V is volume of NaOH (L), M is the mass of GWTW (g) and C_f is SG dye concentration in solvent (mg L^{-1}).

2.10. Modeling of adsorption kinetics and equilibrium

The SG dye adsorption kinetic data were tested and discussed by using different models such as pseudo-first-order model (Lagergren, 1898; Eris and Azizian, 2017; Tan and Hameed, 2017), pseudo-second-order model (Ho and McKay, 1999; Blanchard et al., 1984; Azizian, 2004; Haerifar and Azizian, 2013; Hubbe et al., 2019), Elovich model (Roginsky and Zeldovich, 1934), hyperbolic tangent kinetic model (Eris and Azizian, 2017), modified Lagergren model

(Shahwan, 2015) and diffusion-chemisorption kinetic model (Sutherland and Venkobachar, 2010) (Supplementary material).

The equilibrium sorption behavior of SG dye on GWTW was modeled by the Langmuir (1918), Freundlich (Freundlich, 1906; Tran et al., 2017), Langmuir-Freundlich (Sips, 1948; Azizian et al., 2018; McKay et al., 2014), Koble-Corrigan (Koble and Corrigan, 1952; Foo and Hameed, 2010), Redlich-Peterson (Redlich and Peterson, 1959; Wang and Guo, 2020), Temkin (Temkin and Pyzhev, 1940; Foo and Hameed, 2010; Deng and Ting, 2005) and Toth models equations (Toth, 1971; Wang and Guo, 2020) (Supplementary material).

2.11. Error functions

Non-linear analysis of isotherm models was performed using the Solver add-in, Microsoft Excel (Hossain et al., 2013). The fitness models was signified by the coefficient of determination R^2 from Eq. (5):

$$R^2 = 1 - \frac{\sum_{n=1}^{n} \left(q_e - q_{e,\,model}\right)^2}{\sum_{n=1}^{n} \left(q_e - q_{e,mean}\right)^2} \tag{5}$$

Standard error of an estimate (*SE*) can be defined according to Eq. (6):

$$SE = \sqrt{\frac{1}{m-p} \sum_{i=1}^{m} \left(q_{e,\,exp} - q_{e,calc}\right)^2} \tag{6}$$

where m is the number of experimental points and p is the number of model parameters (Kaludjerovic-Radoicica and Raicevic, 2010).

The nonlinear Chi-square (χ^2) test was used to evaluate the differences between the experimental data and the data calculated from isotherm models. Chi-squared statistic, χ^2:

$$\chi^2 = \sum_{i=1}^{n} \frac{\left(q_{exp} - q_{cal}\right)^2}{q_{cal}} \tag{7}$$

3. Results and discussion

3.1. Characterization of the GWTW

3.1.1. SEM, TEM and EDS analysis

The surface morphology and chemical composition of the GWTW before and after SG dye adsorption were examined by SEM, TEM and EDS. SEM images reveal the structure GWTW powder and the shape of particles. As we can see in Figure 1a, GWTW powder is composed of agglomerated spherical nanoparticles of 50–96 nm. No significant changes on GWTW surface were observed after the contact with SG dyes molecules. The adsorption of SG dye on GWTW was confirmed by EDS. Elemental distributions for five sites of GWTW and SG dye loaded GWTW samples for Fe, O, Si, Ca, P, S, Mn, Mg, Cl and Cr atoms were assessed. In the EDS spectra of GWTW after loading with SG dye the peak characteristic of Cr appeared (Figure 1S). Additionally, weight fraction of P, S and Cl increased but the content (w %) of Ca, Si, Mn and Mg decreased (Table 1, Figure 2S).

Transmission Electron Microscopy (TEM) of the samples was also used to describe the morphology and size of GWTW particles (Figure 1b). As can be seen from GWTW image obtained by TEM (Figure 1b), the adsorbent has a porous surface with the particles size ranging from 40 to 90 nm.

3.1.2. N_2 adsorption-desorption analysis

The nitrogen adsorption–desorption isotherms of GWTW before and after the dye adsorption are shown in Figure 2. They exhibited similarly shaped curves, but the amount of N_2 adsorbed on GWTW after the dye adsorption was slightly higher than that taken up by plain GWTW. According to International Union of Pure and Applied Chemistry (IUPAC) classification (Thommes et al., 2015), GWTW samples before and after adsorption display a type IV(a) isotherm with an H3-type hysteresis loop in the high relative pressure range of 0.45–0.98 P/P_0 (Figure 2). This isotherm is commonly exhibited by many mesoporous industrial adsorbents and inorganic oxide xerogels (Thommes et al., 2015). The plots of pore size distributions, as shown in inset in Figure 2, are located in the mesoporous and macroporous range confirming the mesoporous-macroporous structure of GWTW. The pore size distributions of the GWTW samples are both rather wide, ranging approximately from 3 nm to 120 nm. There is one large peak centered at about 65 nm for the plain GWTW sample (Figure 2). The BET-specific surface area of GWTW before and after the dye adsorption was 34.76 and 43.48 $m^2\,g^{-1}$, respectively (Table 2). The increase in BET surface area and in the mesopore volume was observed following the SG dye adsorption (Table 2). This may be the result of decreased size of GWTW particles during mechanical adsorption system mixing.

3.1.3. FTIR analysis of GWTW and SG dye

FTIR spectroscopy studies were conducted to compare the properties of GWTW before and after the SG dye adsorption. The Fourier transform infrared (FTIR) spectra of GWTW, SG dye and GWTW after the dye adsorption are presented in Figure 3. The FTIR spectrum of GWTW showed the bands at 3300 and 1636 cm^{-1} which can be assigned to the H-bonded O–H stretching modes and H–OH bending vibration of the free adsorbed water, respectively (Chao et al., 2018; Szostak and Banach, 2019; Yoon et al., 2005). Strong band at 957 cm^{-1} with shoulders at 1077 and 850 cm^{-1} comes from bending vibration of FeOH modes (Ociński et al., 2016; Chao et al., 2018). Band at 1000 cm^{-1} is also characteristic of Si–O–Si tetrahedral groups of quartz (Launer, 2013; Chao et al., 2018; Ociński et al., 2016). The peak at 1390 cm^{-1} was assigned to the C–O

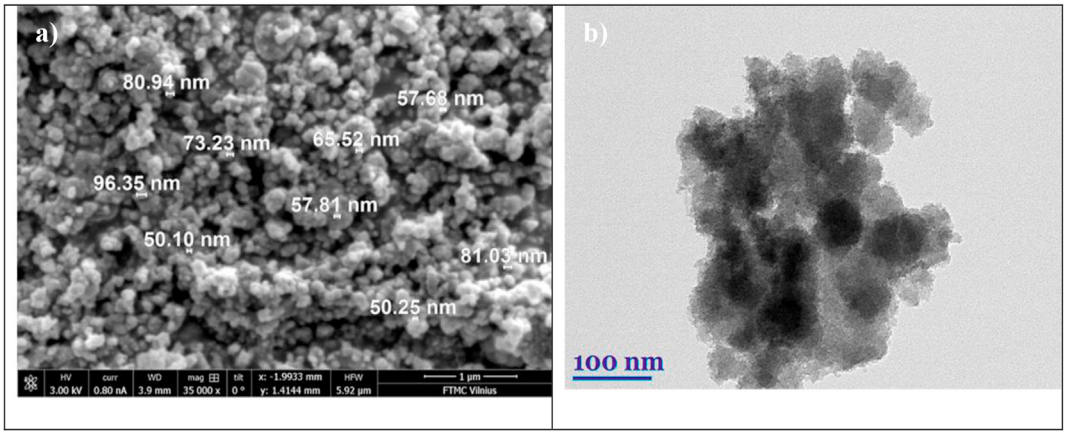

Figure 1. a) SEM of GWTW before SG dye adsorption. b) TEM image of GWTW nanoparticles.

Table 1. EDS analysis data of GWTW before and after SG dye adsorption.

Elements	Before	After
	w %	w %
O	46.02	46.57
Fe	42.85	41.73
Ca	4.570	0.056
P	3.002	5.424
Si	2.740	1.612
S	0.297	2.322
Mn	0.280	0.036
Mg	0.252	0.016
Cl	0.005	1.518
Cr	0.005	0.714

bond in carbonates (Ociński et al., 2016; Zhang and Jia, 2018; Chao et al., 2018; Yoon et al., 2005). The band at 670 cm^{-1} comes from O–Fe–O vibrations (Chao et al., 2018).

For the characterization of SG dye, FTIR spectrum was also studied. Peak positions are at 3307, 2361, 2342, 1579, 1472, 1390, 1271, 1145, 1026, 825 and 737 cm^{-1}. The small peak at 737 cm^{-1} shows Cr–O group, which is inherent by chromium complex compounds (Yildiz and Boztepe, 2002). The intence band at 3307 is due to O–H stretchings (Arami et al., 2008). Intense bands at 1145 and 1026 belong to stretching vibrations of sulfonate groups (Furer et al., 2020; Usman et al., 2019). The bands due to the aromatic ring absorption appears at 1472, 1579 and 1617 cm^{-1} (Usman et al., 2019). Azo bond (N=N) stretching vibrations appear at range 1511–1550 cm^{-1} (Ahmed et al., 2016) and at 1390 cm^{-1} (Nassar, 2010; Coates, 2000). Bands at 825 and 737 can be assigned to C–H out of the plane bending on an aromatic ring (Ahmed et al., 2016).

The Figure 3 also shows the FTIR spectrum of GWTW after the SG dye adsorption. For the dye doped GWTW, the peak at 3300 had shifted to 3283 which might indicate dye interaction with the –OH groups of GWTW. Additionally, the signals characteristic to organic dye with noticeable shifts occurred in the spectrum of GWTW with wave numbers of 1586, 1290 and 1020. Disappear absorption bands at 1472 and 1145 cm^{-1}.

3.1.4. XPS analysis of GWTW and SG dye

XPS analysis was performed to investigate the state and elemental composition of the GWTW surface before and after the dye adsorption. The XPS full-survey spectrum of GWTW sample before SG dye adsorption verified the presence of O, Fe and C elements (Figure 4a). Also, minor amounts of Si, P and Ca were detected. The surface of SG dye doped GWTW additionally contained S, N, Cl and Cr confirming the successful adsorption of SG dye (Figure 4a). The high resolution XPS spectra of Fe, O, Cr and Ca are presented in Figures 4b, c, d and 3S, respectively.

The Fe 2p spectrum of GWTW before adsorption (Figure 4b) had two main peaks of Fe $2p_{3/2}$. They are located at 710.5 eV and 712.3 eV, which correspond to binding energies of the α-Fe_2O_3 (hematite) and Fe(OH)O (goethite, lepidocrocite) phases, respectively (McIntyre and Zetaruk, 1977; Grosvenor et al., 2004). The splitting between the O 1s (Figure 4c) and Fe $2p_{3/2}$ peaks in the XPS spectra serves as a reliable measure of the iron oxidation state. The initial binding energy (BE) of O 1s and BE of Fe $2p_{3/2}$ splitting is equal to 181 eV, revealing Fe^{3+} as the main oxidation state of iron in the GWTW (Hadnadjev et al., 2008). After SG dye adsorption, the shifts of about 1 eV of the Fe $2p_{3/2}$ peaks towards a higher binding energy (711.37 eV and 713.35 eV) were observed. This confirmed that Fe–O and Fe–OH groups acted as the adsorption sites. Slight shifts of the Fe $2p_{3/2}$ and Fe $2p_{1/2}$ peaks towards a higher binding energy were also found earlier by Zhang et al. (2019) for the ferric water treatment residuals after the adsorption of vanadium.

The O 1s spectrum (Figure 4c) of raw GWTW was fitted to four peaks at 529.5 eV, 530.54 eV, 531.6 eV and 532.9 eV, corresponding to Fe–O bonding, Fe–OH bonding, and C–O bonding or chemically/physically adsorbed water (McIntyre and Zetaruk, 1977; Grosvenor et al., 2004;

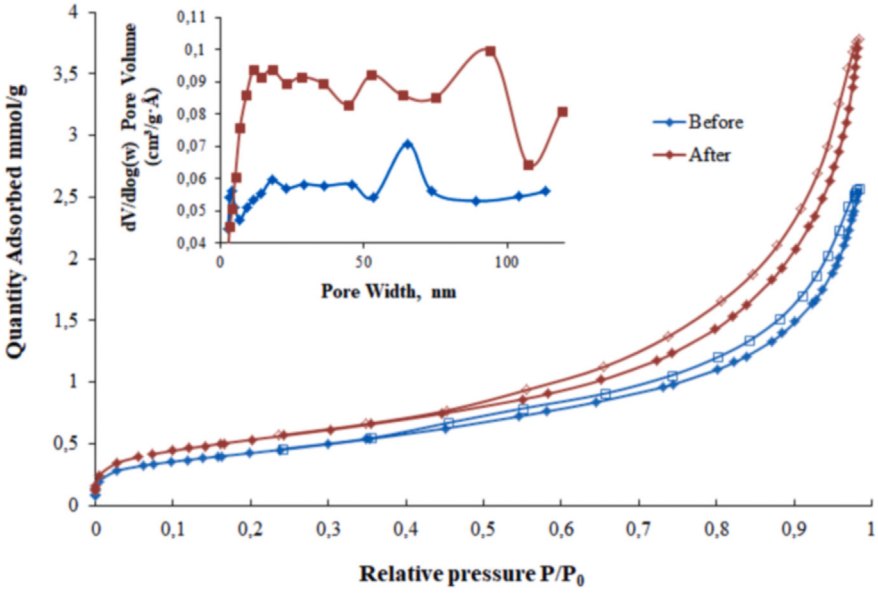

Figure 2. Nitrogen adsorption (full symbols)-desorption (empty symbols) isotherms and pore size distribution plots (inset) of GWTW samples before and after SG dye removal.

Table 2. Textural properties of the GWTW samples before and after Sanodure Green LWN dye adsorption.

Sample	S_{BET} (m^2 g^{-1})	V_{meso} (cm^3 g^{-1})	4 V/S_{BET} (nm)
GWTW	34.7582	0.091305	9.53134
GWTW after SG dye adsorption	43.4809	0.133468	11.34002

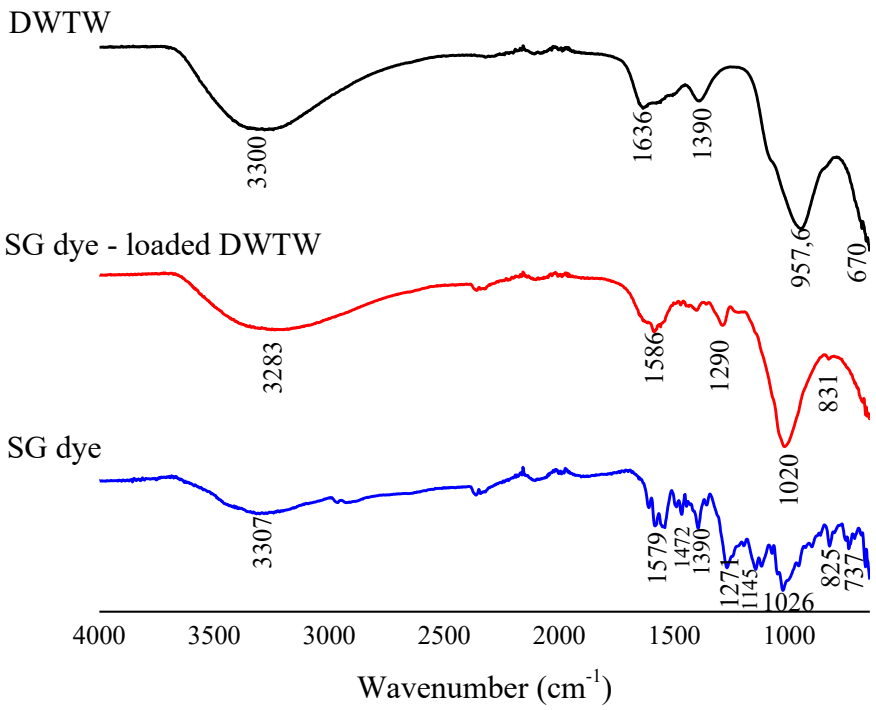

Figure 3. FTIR spectra of SG dye and GWTW before and after SG dye adsorption.

Condi de Godoi et al., 2013; Leiviskä et al., 2019). The BE of 532.9 eV is also characteristic of the oxygen-silicon bonding in SiO_2. The O 1s spectrum of SG dye adsorbed GWTW shows that BE of oxygen of the hydroxy group decreased after the dye adsorption. This change can be due to the interaction between the hydroxyl groups of GWTW and SG dye anions (Zhang et al., 2019). There are two peaks in high – resolution Ca 2p spectra (Figure 3S) at 347.52 ($2p_{3/2}$) and 351.22 eV ($2p_{1/2}$), which can be attributed to $CaCO_3$ (Li and Zeng, 2012; Ni and Ratner, 2008).

The chemical composition of the SG dye was also examined by XPS. The XPS full-survey spectrum of dye sample reveals that C, O, N, S, Na, Cr and Cl are the predominant elements (Figure 4S). The peaks in high-resolution XPS spectra of Cr 2p at BE of 576.4 and 577.85 eV correspond to Cr(III) (Figure 4d) (Chao et al., 2018). In SG dye spectrum, the convolution of S 2p region (Figure 5S) into two peaks of 168.2 eV and 169.43 eV correspond to the sulphur within sulphonate and sulphate, respectively. The BE of S 2p didn't change significantly after the dye adsorption on the surface of GWTW.

Characterization of GWTW by SEM, TEM, EDS, XPS and FTIR proved that the studied adsorbent is environmentally friendly nanomaterial with physical properties and functional groups suitable for interaction with anionic metal complex dye. EDS, FTIR and XPS analysis of GWTW confirmed the successful adsorption of SG dye and showed the dye interaction with the –OH groups of adsorbent.

3.2. Kinetic studies

3.2.1. Modeling of adsorption kinetics

By conducting experiments and modeling the experimental data using various kinetic models, we investigated the influence of SG dye solution concentration, GWTW dosage, pH and temperature on the adsorption rate. The best agreement between the fitted equations and experimental data was obtained for both hyperbolic tangent and diffusion-chemisorption kinetic models, whereas the pseudo-first-order and pseudo-second-order models were less appropriate (Figure 5, Table 3). The Elovich equation was also convenient to describe experimental data. The sorption of metal complex dyes onto pine sawdust particles was also successfully interpreted by the Elovich equation (Özacar and Şengil, 2005). The applicability of the Elovich model in the case of SG dye adsorption by GWTW suggests it is a heterogeneous diffusion process (Xie et al., 2018).

3.2.2. The influence of SG dye concentration

Figure 6 shows the impact of the initial SG dye concentration on the retention rate of adsorbate onto GWTW at increasing contact time.

It is clear that the initial adsorption rate, which can be recognized by the slope of kinetic curves, and the adsorption capacity for the dye enhances by increasing the initial SG dye concentration. By increasing the initial dye concentration from 168 to 635 mg L^{-1}, the amount of SG dye adsorbed during the first 3 min increases from 21 mg g^{-1} to 62 mg g^{-1} (Figure 6). By increasing the contact time, the adsorption capacity was increased. However, with the initial concentration of 345 mg L^{-1} up to 70 % of the dye has been already removed from the solution after 10 min and almost 86 % after 60 min. When the initial concentration was 495 mg L^{-1}, during the first 10 min, about 68 % of the dye was adsorbed and after 60 min contact the color and chromium removal percentage of 85 % was achieved. The stability of GWTW suspension in acidic aqueous solution due to positively charged particles is favorable for the fast achieving of SG dye adsorption equilibrium (Mikhaylov et al., 2016). After increasing of the initial dye concentration to 635 mg L^{-1}, the removal efficiency within the contact of 10 min decreased to 64 % whereas after 60 min contact it was almost the same and reached 83 %. As we can see from Figure 6, the SG dye solutions even with high initial concentration (495–635 mg L^{-1}) can be decolorized successfully during a short time. This can be interpreted by the aggregation of the SG dye molecules in liquid and solid phases (Dias Monte Blanco et al., 2017; Walker and Weatherley, 2001). Self-aggregation of anionic dye molecules is promoted in acidic environment due to dye protonation processes (Moghaddam et al., 2010).

Based on the modified Lagergren equation, SG dye adsorption rate constants and the half-life times ($t_{1/2} = \ln 2/k_1$) were calculated and compared (Table 3). We can see that the half-life times obtained from both color and chromium content reduction measurements, are similar ranging from 2.8 to 7.4 min (Table 3, Table 5S). The adsorption half-life time increases with increasing in initial dye concentration. By using

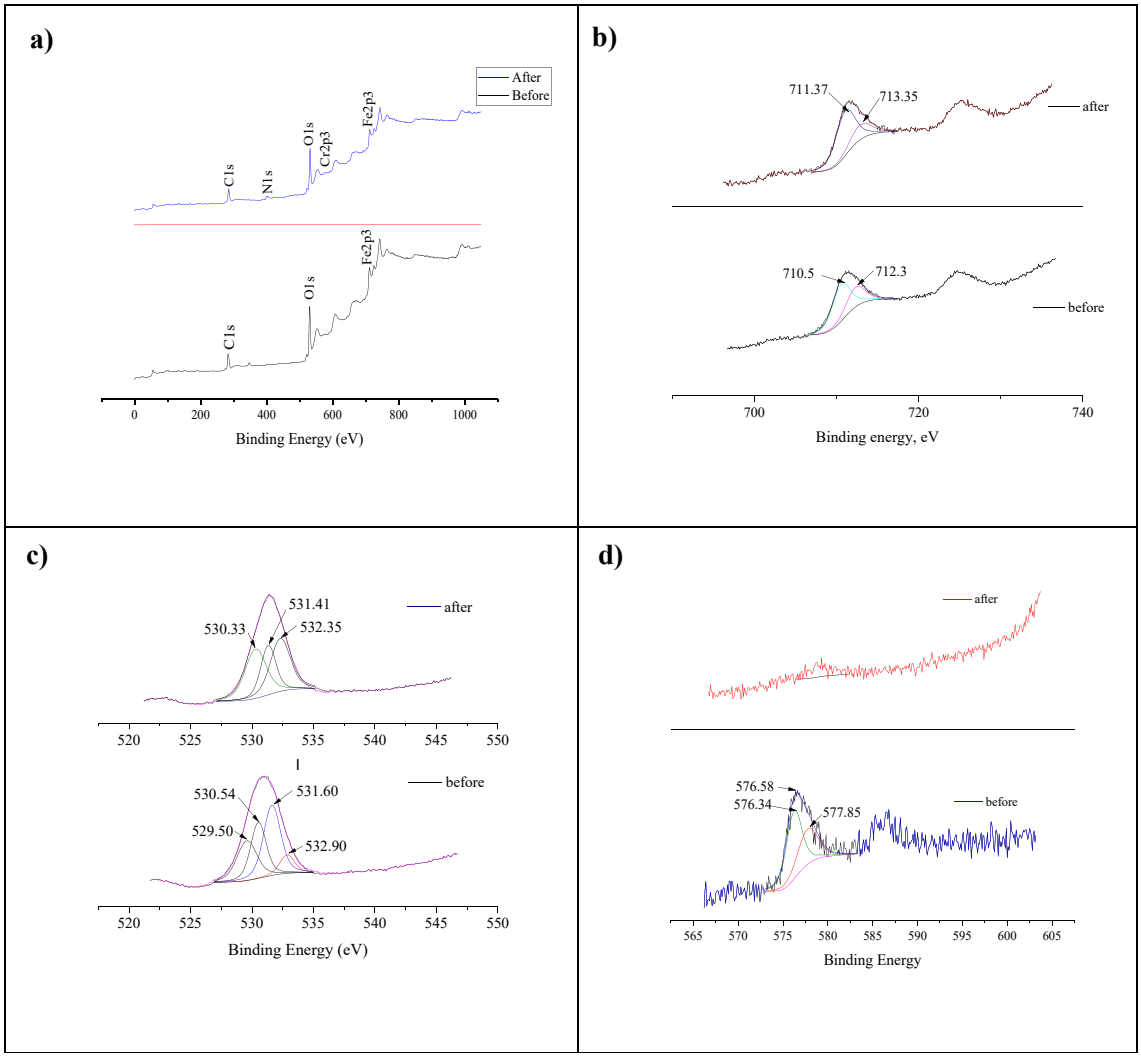

Figure 4. The XPS survey of GWTW before and after SG dye adsorption (a); the high-resolution XPS spectra of Fe 2p of GWTW before and after SG dye adsorption (b); O 1s of GWTW before and after SG dye adsorption (c); Cr 2p within SG dye and GWTW doped with SG dye (d).

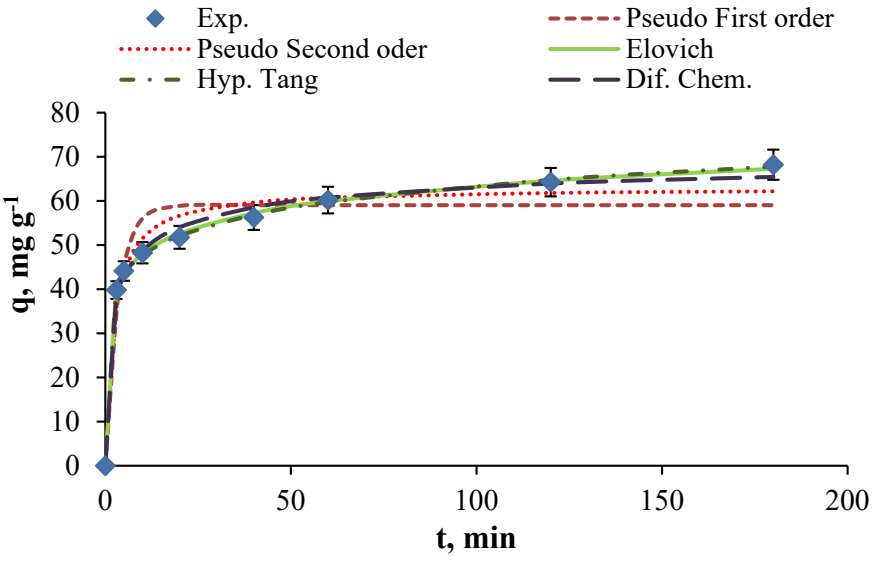

Figure 5. Kinetic experimental data and modeling for the adsorption of SG dye by GWTW. Conditions: C_0 = 345 mg L^{-1}, pH = 2, T = 20 °C, adsorbent dose 5 g L^{-1}.

Table 3. Kinetic parameters for the effect of SG dye concentration on adsorption by GWTW.

Concentration of SG dye, mg L^{-1}				
Parameters	168.0	345.0	495.0	635.0
Pseudo-first order model				
q_e, ($mg{\cdot}g^{-1}$)	29.18	59.02	84.82	102.4
k_1 (min^{-1})	0.380	0.297	0.258	0.233
R^2	0.9660	0.9214	0.9267	0.9252
SE	2.178	6.075	8.462	10.381
Pseudo-second order model				
q_e ($mg{\cdot}g^{-1}$)	31.31	62.93	90.76	110.0
k_2 ($mg^{-1}{\cdot}g{\cdot}min^{-1}$)	0.020	0.007	0.004	0.003
R^2	0.9901	0.9690	0.9745	0.9754
SE	1.176	3.819	4.996	5.956
Elovich model				
A ($mg{\cdot}g^{-1}{\cdot}min^{-1}$)	613.0	871.2	655.0	502.4
B ($g{\cdot}\ mg^{-1}$)	0.291	0.150	0.096	0.075
R^2	0.9994	0.9990	0.9993	0.9994
SE	0.272	0.693	0.846	0.957
Hyperbolic tangent model				
q_e ($mg{\cdot}g^{-1}$)	38.86	76.41	110.7	135.9
t_{eHT} (min)	110	132	167	191
n_{HT}	0.164	0.180	0.202	0.229
R^2	0.9928	0.9941	0.9996	0.9992
SE	0.999	0.999	0.997	1.000
Modified Lagergren model				
Q_{max}, ($mg{\cdot}g^{-1}$)	33.61	68.93	98.76	127.00
k_1 (min^{-1})	0.248	0.184	0.163	0.119
$t_{1/2}$ (min)	2.8	3.8	4.2	7.4
R^2	0.9517	0.7835	0.8005	0.6781
SE	3.759	9.432	13.065	20.148
Diffusion – chemisorption model				
q_e ($mg{\cdot}g^{-1}$)	36.51	73.15	107.1	131.8
K_{DC} ($mg\ (g{\cdot}min^{0.5})^{-1}$)	28.97	46.21	59.24	64.30
k_i	22.99	29.19	32.77	31.36
R^2	0.9979	0.9931	0.9961	0.9975
SE	0.539	1.803	1.949	1.901

diffusion-chemisorption kinetic model, the SG dye removal rate constants were calculated. It was observed that the rate constants increase with increasing initial dye concentration. The linear dependence of K_{DC} on C_0 was revealed and depicted in Figure 6S (Supplementary material). The same trend was obtained by Sutherland and Venkobachar (2010). Additionally, the initial SG dye removal rates were calculated. We have observed that the initial rates of diffusion-chemisorption of SG dye molecules were higher from the solutions with higher initial concentration. This may be explained with the increased dye concentration gradient. Hyperbolic tangent model enables to determine the time

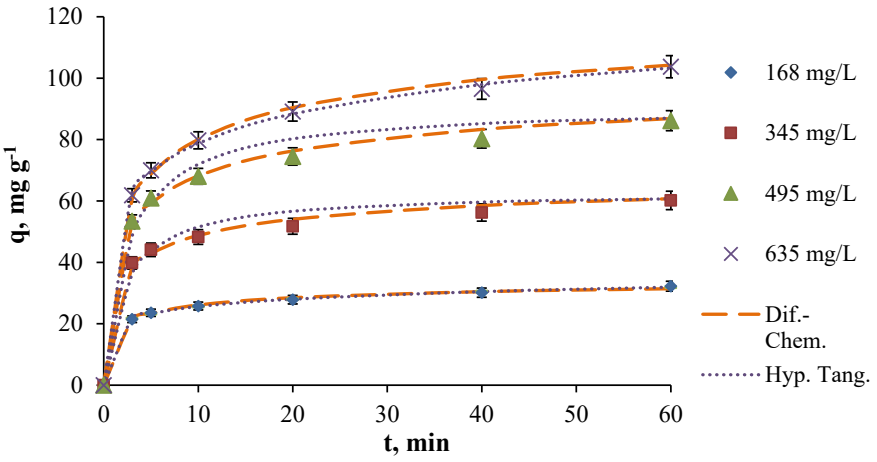

Figure 6. Effect of contact time on SG dye adsorption capacity by GWTW for various initial concentrations. Conditions: pH = 2, T = 20 °C, adsorbent dose 5 g L^{-1}. The points represent experimental data; the lines represent diffusion-chemisorption and hyperbolic tangent models.

needed to attain equilibrium (Eris and Azizian, 2017). As shown in Table 3 the adsorption of SG dye reaches equilibrium after 110–190 min depending on initial dye concentration.

3.2.3. Effect of pH

The experimental studies revealed that the removal efficiency was sensitive to SG dye solution pH. The effect of initial pH was tested by using 150 mg L^{-1} SG dye solutions with pH values from pH 1.5 to pH 4.0. An increasing of initial pH from 2.0 to 3.0 leads to a significant decrease of SG dye adsorption capacity from 34 mg g^{-1} to 7 mg g^{-1} for 20 min contact, whereas the retention of chromium during the same period of time decreased from 0.77 to 0.20 mg g^{-1} (Figure 7S). The influence of solution pH might be related to the protonation of GWTW surface according to (8) equation (Cornell and Schwertmann, 2003; Aredes et al., 2013; Ahmed et al., 2013):

$$=FeOH + H^+ \leftrightarrow = FeOH_2^+ \quad (8)$$

Similarly, the surface hydrolysis reaction for goethite was described as follows (Jeppu and Clement, 2012):

$$> FeOOH + H^+ \leftrightarrow FeOOH_2^+ \quad (9)$$

The surface of GWTW acquires positive charge by adsorbing H^+ ions. Due to the positive surface charge of GWTW, the negative SG dye molecules can be effectively attracted:

$$=FeOH + A^{2-} + H^+ \rightarrow = FeA^- + H_2O \quad (10)$$

$$=FeOH + A^{2-} + 2\,H^+ \rightarrow FeHA + H_2O \quad (11)$$

The evidence of GWTW –OH groups' interaction with the dye molecules was supported by the results of FTIR and XPS analysis. Therefore, it can be concluded that electrostatic interaction is the main mechanism of the SG dye removal. Electrostatic attraction is stronger when the density of positive surface charge is higher. A decrease of $[H^+]$ in the SG dye solution will be followed by the decrease in positive GWTW surface density and adsorption capacity of GWTW. We have detected that the pH values during the SG dye removal process only slightly changed in strongly acidic solutions, whereas a significant increase in solution pH was observed using SG dye solutions initially acidified to pH 3 or pH 4. The increase of solution pH was not favorable for the uptake of SG dye molecules. This is understandable since the zeta potential of GWTW measured in the SG dye solution with pH 5.6 was negative (-17.7 ± 0.5 mV). As we can see from Figures 7 and 8S, the removal efficiency of SG dye color after the 20 min of contact with GWTW reached up to 90 % in the solutions with initial pH value 1.5 and 2.0, whereas it decreased to 23 % and 19 % in the solutions with the initial pH 3.0 and 4.0, respectively (Figures 7 and 9S). Adsorption of SG dye is fast from strongly acidic solutions, and according to the modified Lagergren model, the half-life times of color and chromium removal do not exceed 2.2–2.3 min. The dye removal rate constants of diffusion-chemisorption kinetic model are about three-fold higher for the solutions with initial pH values 1.5 and 2.0 compared to those for the solutions with the initial pH 3 and 4 (Table 2S).

Additionally, experiments have been performed to investigate the extent of iron and calcium leaching from GWTW in the acidic environment. The ICP-OES analysis of SG dye solutions after the contact with GWTW showed that the iron leaching intensity increased from 0.30 to 43 mg L^{-1} as the initial pH value was decreased from 4.0 to 1.5 (Figure 7). The action of Fe^{3+} ions as coagulation agent produced in the acidic dye solutions is favorable for color removal. The possible mechanism could be neutralization of negative charges of anionic dye by Fe^{3+} ions and their hydrolysis products (Moghaddam et al., 2010; Cornell and Schwertmann, 2003). The transfer of positive Ca^{2+} ions from GWTW to SG dye solution during the contact with GWTW (Figure 7) can also facilitate the dye removal process due to their interaction with negatively charged SG dye anions. Ca^{2+} cations may bridge between sulfonate groups ($-SO_3^-$) of SG dye and negatively charged sites of GWTW (Najafpoor et al., 2016). Another possible explanation of the positive effect of calcium ions on the dye removal may be the dye aggregation. Powdered activated carbons also showed better removal efficiency for reactive Blue 81 dye after modified with calcium (Lv et al., 2020).

3.2.4. Effect of temperature

It is well known that changing the temperature changes the kinetic properties of adsorbate and adsorption capacity of adsorbent. Temperature influenced the viscosity of SG dye solution and the rate of diffusion of the dye molecules across the boundary layer and in the mesopores and macropores of the GWTW particles. On the other hand, with increasing temperature, the attractive forces between GWTW surface and the dye molecules are weakened. Additionally, the rise of temperature may change the desorption rate through the enlarged mobility of SG molecules. An increase of temperature lowers the dye aggregation number (Navarro and Sanz, 1999). We performed the SG dye adsorption experiments at three different temperatures of 20, 40 and 60 °C. Figure 8 shows the reduction of chromium concentration in SG dye solution as time proceeds. The same trend was observed during UV-vis absorbance measurements. The experimental results imply that the increase in temperature leads to the worse dye removal and that the SG dye adsorption process by GWTW is exothermic in nature. For all temperatures tested, the percent dye removal was highest at the beginning of the process but the difference between adsorption rates was more noticeable after 10 min (Figure 8). The kinetic parameters for the effect of temperature on SG dye and chromium removal by GWTW are presented in Table 3S and Table 7S, respectively.

3.2.5. Effect of the GWTW dose

The determination of the optimal dose of adsorbent is necessary to clarify the conditions under which the highest removal efficiency could be achieved. The effect of GWTW dosage on SG dye removal was investigated without the correction of solution pH during the adsorption process to ascertain the optimal ratio of H^+ ions concentration to adsorbent mass in adsorption systems. Earlier we have already determined (Zubrytė et al., 2019) that the suspension of GWTW in deionized water was basic (pH = 8 at the W/V ratio 1:100) due to reactions (Hedricks, 2006):

$$Fe(OH)_3 \leftrightarrow Fe^{3+} + 3\,OH^- \quad (12)$$

$$FeOOH + H_2O \leftrightarrow Fe^{3+} + 3\,OH^- \quad (13)$$

$$CaCO_3 \leftrightarrow Ca^{2+} + CO_3^{2-} \quad (14)$$

$$CO_3^{2-} + H_2O \leftrightarrow HCO_3^- + OH^- \quad (15)$$

As GWTW acts as Brønsted base, the higher dosage of GWTW requires the higher quantity of acid to maintain the optimal solution pH. The

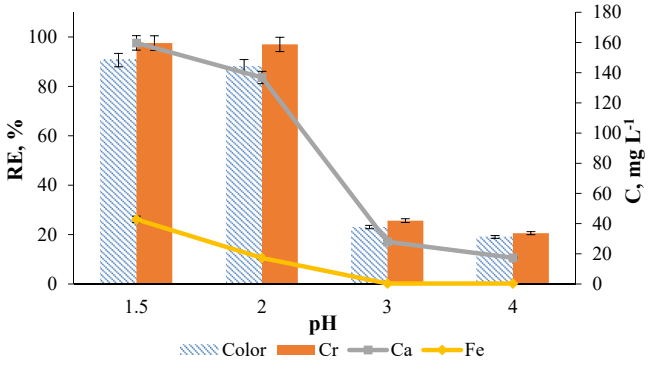

Figure 7. Effect of initial solution pH on the removal efficiency of SG dye and leaching intensity of iron and calcium from GWTW. Conditions: C_0 (SG dye) = 150 mg L^{-1}, T = 20 °C, adsorbent dose 4 g L^{-1}. Contact time 20 min.

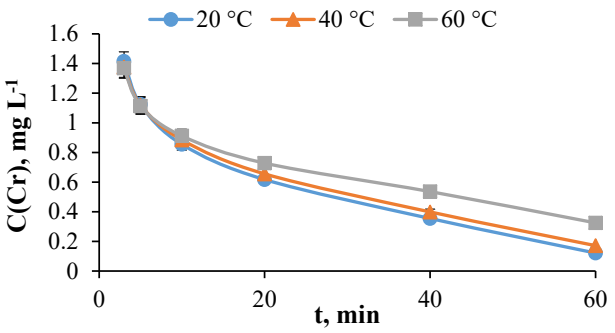

Figure 8. The chromium content decay curves at different temperatures. Conditions: initial chromium concentration 3.94 mg L^{-1}; pH 2, adsorbent dose 5 g L^{-1}.

decrease of SG dye adsorption capacity with increasing in GWTW dose (Figure 9) is not only due to a split of the dye molecules on higher adsorbent surface but also due to the rise in solution pH and the decrease of positive charge density on the GWTW surface of adsorbent. It was determined that the maximum SG dye removal efficiency could be achieved with the ratio of 2.5 mmol H^+ ions/g adsorbent.

As we can see from Figure 9, the influence of GWTW dosage on SG dye removal is related to the dye solution pH effect. The higher the GWTW concentration in the solution, the more appreciable is the change in solution pH during the course of the dye adsorption. The highest percentage of SG dye removal was obtained with the adsorbent dose 4–5 g L^{-1}. When the initial dye solution pH value was pH_0 = 2 and the adsorbent dose 0.2 g, the removal efficiency was 78 % and about 90 % after 10 min and 40 min contact, respectively. Whereas, when the adsorbent dose of 0.35 g was taken, the removal efficiency decreased to 73 % after 10 min contact and even to 64 after 40 min contact. Obviously, this is a consequence of the solution pH increase from the initial value of pH 2 to pH 4.6 after 10 min and pH 5.5 after 40 min. According to diffusion – chemisorption model, the equilibrium adsorption capacity could be 39.6 mg g^{-1} with the GWTW dosage 4 g L^{-1} whereas only 15.8 mg g^{-1} with the GWTW dosage increased up to 7 g L^{-1} (Figure 9). The kinetic parameters for the effect of GWTW dose on SG dye and chromium removal by GWTW are presented in Table 4S and Table 8S, respectively.

Monitoring of the chemical behavior of adsorption system during the dye removal process leads to the conclusion that the physical state and chemical composition of natural adsorbent GWTW determines the optimal process conditions. Initial dye solution pH should be regulated in accordance to the dosage of adsorbent to attain the optimal and constant pH value in the solution. It is important to note that the dye removal could represent the cost-effective process with the maximum adsorption speed at room temperature for which the pretreatment of adsorbent before use is not required. Additionally, it is suitable for the dye solutions with high initial concentration. The applicability of diffusion-chemisorption model for SG dye - GWTW adsorption system suggests that the color and chromium removal rate is controlled by both the adsorbate diffusion in liquid phase and the pores of adsorbent as well as the interaction at the active adsorption sites. Theoretical models that fitted to the experimental data well enable to determine the effects of initial dye concentration, pH, temperature and adsorbent mass on the kinetic parameters for SG dye adsorption by GWTW.

3.3. Adsorption equilibrium

Adsorption isotherms describe how SG dye molecules interact with the GWTW particles at equilibrium (Figure 10) and are important in optimizing the application of adsorbent (Cheruiyot et al., 2019; Al-Ghouti and Da'ana, 2020). Experimental points presented in Figure 10 show the adsorption capacity q_e and equilibrium SG dye concentration in the liquid phase at a constant solution pH 2 and temperature 20, 40 or 50 °C. Isotherm models can accurately predict the dependence of adsorbent efficiency at equilibrium on the initial adsorbate concentration, adsorbent mass, solution volume and temperature (Kumar et al., 2019).

The parameters of the used models estimated by non-linear method are given in Table 4. They provide some insight into the affinity of SG dye molecules towards GWTW as adsorbent. Figure 10 contains experimental points for SG dye concentrations from 50 to 1000 mg L^{-1} and the equilibrium adsorption curves predicted by Langmuir-Freundlich model. The highest correlation coefficients, the lowest Chi-square values (χ^2) and the standard errors (SE) of q_e for Langmuir-Freundlich isotherm suggest that it is the best model of representing experimental data. The best fit to Langmuir-Freundlich isotherm indicates the heterogeneous nature of adsorption sites on GWTW surface. The source of heterogeneity may be structural and/or energetic properties of GWTW (McKay et al., 2014). According to Langmuir-Freundlich model, the amount of dye removed at equilibrium decreased from 185 to 167 mg g^{-1} with the increase in temperature from 293 to 323 K. Analogously, the adsorption capacity for chromium decreases from 5.5 to 4.1 mg g^{-1} with the increasing temperature from 293 to 323 °C (Figure 11S). The lower adsorption capacity at higher temperature correlates with the decrease of Langmuir-Freundlich isotherm constant K_a which changes from 0.056 to 0.016 as the temperature increases from 293 to 323 K (Table 4). The adsorption capacity for SG dye at 293 K temperature increases from 7.7 to 191 mg g^{-1} with the increasing of initial SG dye concentration from 50 to 1000 mg L^{-1} (Figure 10). The removal efficiency of SG dye evaluated by the residual color is in the range of about 89–95 % (Figure 10S). The degree of chromium retention from the 50 mg L^{-1} SG dye solution was about 92 %, and it only slightly decreased to 87-85 % (Figure 10S) with high initial dye concentration (800–1000 mg L^{-1}).

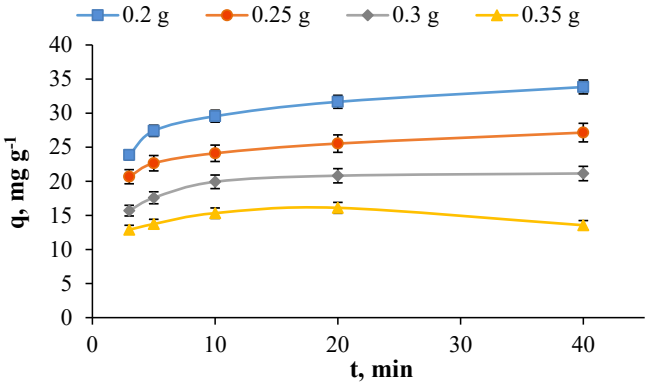

Figure 9. Effect of GWTW dose on SG dye adsorption capacity. Conditions: initial dye concentration 150 mg L^{-1}; pH_0 = 2, T = 20 °C.

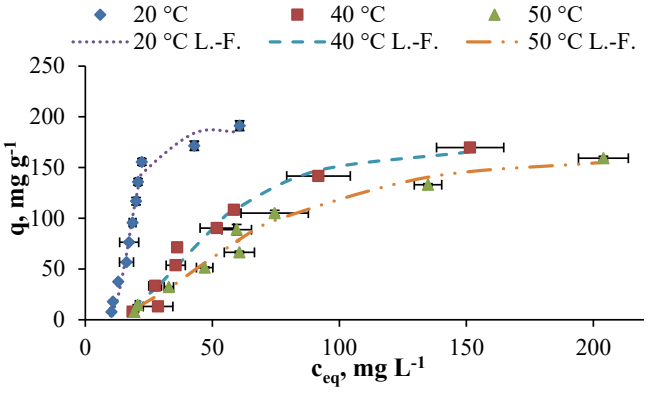

Figure 10. Experimental adsorption isotherms (symbols) and Langmuir-Freundlich model fits (lines) of SG dye on GWTW at different temperatures. Conditions: pH 2, adsorbent dose 5 g L^{-1}, contact time 8 h.

Table 4. Parameters for the equilibrium adsorption of SG dye onto GWTW.

Model	Parameter	Temperature		
		20°C	*40°C*	*50°C*
Langmuir	q_m	495.66	423.98	365.50
	K_L	0.0119	0.0054	0.0041
	R^2	0.7472	0.8854	0.9541
	SE	33.339	24.616	14.676
	χ^2	20.618	17.310	8.4942
Freundlich	K_F	9.0021	3.8550	3.1044
	n	1.2935	1.3091	1.3243
	R^2	0.7149	0.9016	0.9356
	SE	35.411	22.804	17.386
	χ^2	20.994	14.970	9.6146
Langmuir-Freundlich	Q_m	185.16	172.77	166.49
	K_a	0.0556	0.0206	0.0157
	n	5.8525	2.7463	2.2434
	R^2	0.9797	0.9782	0.9862
	SE	9.9986	11.892	8.6710
	χ^2	3.7332	6.1047	2.6329
Kobble – Corrigan	A	1.9999	0.0163	0.0150
	b	0.0055	0.0001	0.0001
	n	1.4043	2.3306	2.2434
	R^2	0.7655	0.9739	0.9862
	SE	34.062	12.692	8.6710
	χ^2	17.504	2.3999	2.6328
Redlich–Peterson	A	5.0337	1.7774	1.2153
	B	0.0028	0.0049	0.0069
	g	1.2360	0.9102	0.7723
	R^2	0.7469	0.9189	0.9347
	SE	32.735	22.366	18.913
	χ^2	19.849	12.966	8.6524
Temkin non-linear	A	0.1128	0.0547	0.0555
	B	125.07	84.438	65.662
	R^2	0.8347	0.9713	0.9800
	SE	26.957	12.319	9.6760
	χ^2	7.9711	7.5257	3.6331
Toth	k_T	0.0272	0.0093	0.0076
	q_T	186.03	170.50	162.70
	t	7.7530	8.8291	4.1040
	R^2	0.7957	0.9157	0.9518
	SE	31.789	12.272	7.1614
	χ^2	19.725	12.273	7.1613

A higher equilibrium binding constant of Temkin isotherm at 293 K temperature indicates a higher GWTW adsorption potential at ambient temperature (Table 4). Based on Toth model, the higher value of K_t at lower temperature also means the higher adsorption affinity (Table 4). The largest K_F value of Freundlich isotherm constant at 293 K temperature is in accordance with higher adsorption capacity of GWTW for SG dye at room temperature when compared to elevated temperature adsorption. The parameters of the used models for chromium are given in Table 9S.

3.4. Thermodynamic evaluation of SG dye removal

Langmuir-Freundlich model constants were used for the thermodynamic evaluation of SG dye adsorption by GWTW. Thermodynamic parameters (the change in standard enthalpy, the change in standard entropy and Gibbs free energy) can be determined from the following equations (Atkins and de Paula, 2010):

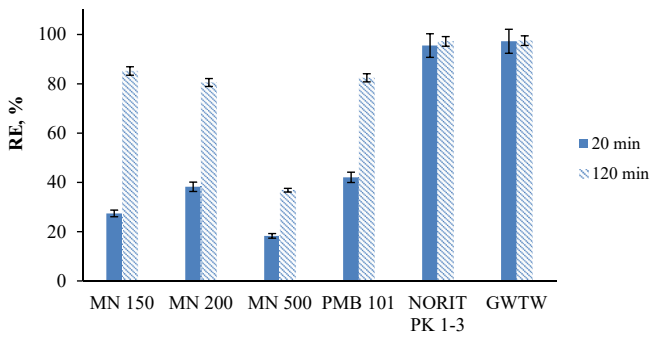

Figure 11. Comparison of the efficiency of different adsorbents in the removal SG dye. Conditions: SG dye solution pH 2, adsorbent dose 4 g L^{-1}, temperature 20 °C, contact time 20 and 120 min.

Table 5. The values of thermodynamic parameters for the adsorption of SG dye by GWTW.

Temperature (K)	$K_e°$	ΔG° (kJ mol^{-1})	ΔH° (kJ mol^{-1})	ΔS° (J mol^{-1}·K^{-1})	Van't Hoff equation
293	4.726·10^4	-26.26	-35.80	-32.56	y = 4307x-3.916
313	1.751·10^4	-25.62			R^2=0.984
323	1.335·10^4	-25.29			

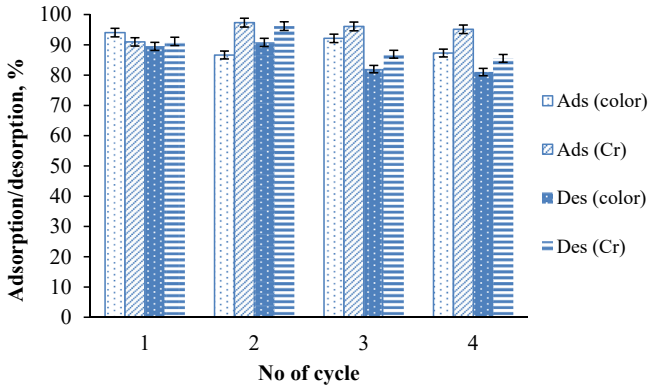

Figure 12. The adsorption - desorption cycles for the removal of SG dye by GWTW using 0.05 M NaOH as eluent.

$$\Delta G^0 = -RT\ln\left(K_e^\circ\right) \tag{16}$$

$$\ln\left(K_e^\circ\right) - \frac{\Delta H^0}{R} \cdot \frac{1}{T} + \frac{\Delta S^0}{R} \tag{17}$$

where R is the universal gas constant (8.314 J K^{-1} mol^{-1}), T is the absolute temperature (Kelvin), K_e° is the thermodynamic equilibrium constant, ΔH° is the change in standard enthalpy (J mol^{-1}), $\Delta S°$ is the change in standard entropy (J K^{-1} mol^{-1}) and $\Delta G°$ (J mol^{-1}) is the change in standard free Gibbs energy.

The thermodynamic equilibrium constants K_e° were calculated by using equation (Lima et al., 2019):

$$K_e^\circ = \frac{(1000 \cdot K_g \cdot molecular\ weight\ of\ adsorbate)[Adsorbate]^\circ}{\gamma} \tag{18}$$

where γ is the coefficient of activity (dimensionless), *[Adsorbate]*° is the standard concentration of the adsorbate (1 mol L^{-1}), K_g is Langmuir-Freundlich equilibrium constant (L mg^{-1}) and $K_e°$ is the thermodynamic equilibrium constant (dimensionless). The conversion of L mg^{-1} into L g^{-1} is obtained by the multiplication of the value of K_g (L mg^{-1}) by 1000.

By constructing a plot of ln(K_e°) versus *1/T* (Figure 12S), it is possible to determine the change in enthalpy (ΔH°) and the change in entropy ($\Delta S°$) from the slope and the intercept of the graph, respectively. The values of ΔH°, ΔS° and $\Delta G°$ are presented in Table 5. According to thermodynamic calculations, the process of SG dye adsorption was exothermic ($\Delta H^\circ = -35.80$ kJ mol^{-1}, Table 5). The exothermic nature of Congo red dye adsorption by cashew nut shell was also determined by Senthil Kumar et al. (2010). The value of enthalpy change indicates the physisorption with an electrostatic interaction of GWTW with the dye. The change of enthalpy for electrostatic interaction as a kind of physisorption varies from 20 to 80 kJ mol^{-1} (Machado et al., 2014).

The sign of ΔH is in compliance with experimental data of the SG dye adsorption isotherms demonstrating lower adsorption capacity (q_e) at higher temperature (Figure 10). The negative value of ΔS = -32.56 J mol^{-1}·K^{-1} describes that the more ordered structure at adsorbent/solution interface is obtained as a result of accumulation of SG dye molecules on GWTW. The negative changes in Gibbs free energy indicate the spontaneity of the SG dye removal process. The negative values of ΔG increase with temperature increase, confirming that the adsorption of SG dye is more favorable at a lower temperature.

3.5. Comparison of adsorbents for the removal of SG dye

In addition to natural GWTW adsorbent, five different types of commercially available adsorbent materials were used to compare their efficiency in the removal of SG dye from aqueous solutions. The calculated SG dye removal percentages are presented in Figure 11. As we can see from the data, after 20 min contact of the adsorbents with SG dye solution, the most promising results of the dye removal efficiency were achieved by using GWTW and powdered activated carbon NORIT PK 1–3. Their adsorption capacities were also quite similar after contact time extended to 120 min. The adsorption of SG dye by polymeric adsorbents (anionic MN 150, non-ionic MN 200 and mixed bed PMB 101) during the first 20 min was relatively low. However, the dye removal efficiency increased after 120 min contact and reached more than 80 %. The worst result even over a longer period of time was obtained using MN 500

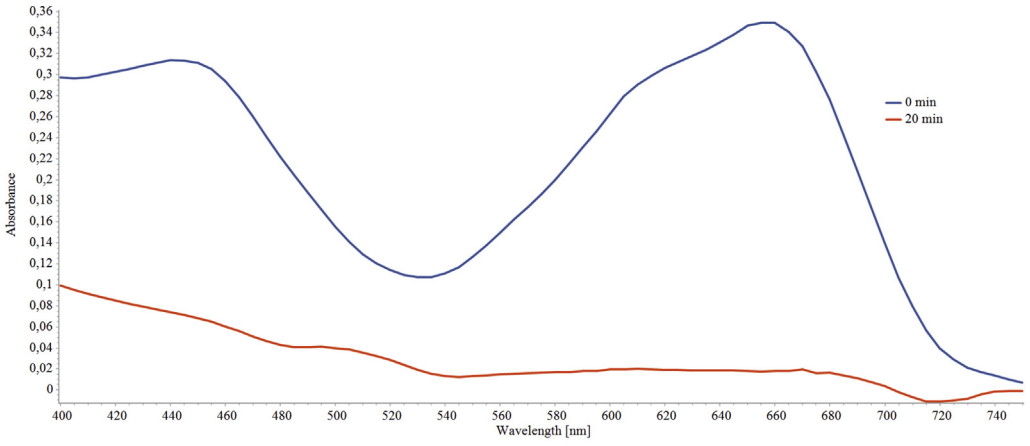

Figure 13. The UV–vis spectra of anodized aluminum dyeing wastewater sample before treatment and after 20 min contact with GWTW (process conditions: pH 2.0–4.4; V/W 17:1; T 20 °C).

cation exchanger. This reaffirms that the dye removal was dominated by electrostatic interaction.

3.6. SG dye desorption study

Reusability of GWTW was evaluated by performing four successive cycles of SG dye adsorption-desorption. Alkaline solution (0.05 M NaOH) was selected as eluent to neutralize the positive surface charge of GWTW and shift the reaction (10) equilibrium to the left. The effect of adsorption-desorption cycle on the SG dye adsorption capacity can be seen in Figure 12. The obtained results indicated that GWTW could be successfully regenerated with NaOH solution and reused without significant decrease in SG dye removal efficiency.

3.7. Real wastewater treatment

The GWTW as adsorbent was implemented for the treatment of real wastewater produced after dyeing of anodized aluminum by adsorption. The initial pH of wastewater was 5.7. It was diminished to pH 2 with the addition of 5 M HCl but after 20 min contact with GWTW (wastewater volume/adsorbent mass ratio 17:1) raised up to 4.4. The color removal efficiency of the real wastewater can be calculated as follows:

$$Color\ removal\ efficiency = 100 \cdot (A_0 - A_t)/A_0 \quad (19)$$

where A_0 and A_t are absorbance values of the wastewater before the treatment and at time t.

The UV–Vis spectra of anodized aluminum dyeing wastewater sample before treatment and after 20 min contact with GWTW are presented in Figure 13. The color removal efficiency of anodized aluminum dyeing wastewater determined by Eq. (19), was about 80 %. Chromium reduction efficiency was calculated according to Eq. (20):

$$Chromium\ reduction\ efficiency = 100 \cdot (C_0 - C_t)/C_0 \quad (20)$$

where C_0 and C_t are chromium concentrations in the wastewater before the treatment and at time t.

ICP – OES analysis has shown that the chromium reduction efficiency of 97 % was attained. The content of aluminum in the treated wastewater was also below the detection limits. The experimental studies disclose that GWTW could be utilized as a low-cost adsorbent in anodized aluminum wastewater treatment for the decoloration and the removal of chromium and aluminum.

4. Conclusions

According to the results of SEM-EDX, TEM, N_2 adsorption/desorption, FTIR and XPS analysis, the groundwater treatment waste (GWTW) can be characterized as an eco-friendly nanomaterial with mesoporous-macroporous structure and with a specific surface area S_{BET} equal to 35 $m^2\ g^{-1}$.

Kinetic studies have showed that the removal process was fast and up to 90 % of the SG dye was removed within a contact time of 20 min from the 150 mg L^{-1} SG dye solution. Adsorbent concentration 4–5 g L^{-1}, 20 °C temperature and solution pH 2 were optimal conditions for the SG dye removal. Kinetic curves at different initial SG dye and GWTW adsorbent concentrations, temperatures and pH fitted well to diffusion-chemisorption, hyperbolic tangent and Elovich models. The adsorption system is strongly affected by pH changes in the solution. When the initial dye solution $pH_0 > 2$, the increase in final pH was observed due to the basic properties of GWTW. The heterogeneous adsorption of SG dye was confirmed by applicability of Langmuir-Freundlich model and the maximum equilibrium capacity at 293 K was 185 mg g^{-1}. SG dye solutions even with high initial concentration (500–600 mg L^{-1}) can be decolorized successfully. Thermodynamic study has showed that the adsorption of SG dye by GWTW was exothermic, spontaneous and with more ordered structure at the interface of the adsorbate and solution. According to magnitude of enthalpy, electrostatic interactions between the positive GWTW surface and the negative dye molecules are involved in pH dependent adsorption process. The presence of ferric and calcium ions in the adsorption system may have the positive effect on the dye removal process. We conclude that GWTW, as an eco-friendly and renewable nanomaterial, can be successfully used for the fast and efficient removal of anodized aluminum dye from acidic aqueous media. The efficiency of GWTW adsorbent was also approved in the treatment of anodized aluminum industry wastewater.

Declarations

Author contribution statement

A. Gefenienė and D. Kaušpėdienė: Analyzed and interpreted the data; Wrote the paper.

E. Sodaitienė: Performed the experiments; Analyzed and interpreted the data.

R. Ragauskas, A. Selskienė, V. Jasulaitienė and J. Vaičiūnienė: Contributed reagents, materials, analysis tools or data.

R. Ramanauskas: Conceived and designed the experiments.

Funding statement

This work was supported by the Ministry of Education, Science and Sport of the Republic of Lithuania.

Data availability statement

Data included in article/supplementary material/referenced in article.

Declaration of interests statement

The authors declare no conflict of interest.

Additional information

Supplementary content related to this article has been published online at https://doi.org/10.1016/j.heliyon.2021.e05993.

References

Ahmed, F., Dewani, R., Pervez, M.K., Mahboob, S.J., Soomro, S.A., 2016. Non-destructive FT-IR analysis of mono azo dyes. Bulg. Chem. Commun. 48, 71–77.

Ahmed, M.A., Ali, S.M., El-Dek, S.I., Galal, A., 2013. Magnetite–hematite nanoparticles prepared by green methods for heavy metal ions removal from water. Mater. Sci. Eng.: B. 178 (10), 744–751.

Al-Ghouti, M.A., Da'ana, D.A., 2020. Guidelines for the use and interpretation of adsorption isotherm models: a review. J. Hazard Mater. 393, 122383.

Arami, M., Limaee, N.Y., Mahmoodi, N.M., 2008. Evaluation of the adsorption kinetics and equilibrium for the potential removal of acid dyes using a biosorbent. Chem. Eng. J. 139, 2–10.

Aredes, S., Klein, B., Pawlik, M., 2013. The removal of arsenic from water using natural iron oxide minerals. J. Cleaner Prod. 60, 71–76.

Atkins, P., de Paula, J., 2010. Physical Chemistry, ninth ed. W. H. Freeman and Company, New York.

Azizian, S., Eris, S., Wilson, L.D., 2018. Re-Evaluation of the Century-Old Langmuir Isotherm for Modeling Adsorption Phenomena in solution.

Azizian, S., 2004. Kinetic models of sorption: a theoretical analysis. J. Colloid Interface Sci. 276, 47–52.

Blanchard, G., Maunaye, M., Martin, G., 1984. Removal of heavy metals from waters by means of natural zeolites. Water Res. 18 (12), 1501–1507.

Castaldi, P., Mele, E., Silvetti, M., Garau, G., Deiana, S., 2014. Water treatment residues as accumulators of oxoanions in soil. Sorption of arsenate and phosphate anions from an aqueous solution. J. Hazard Mater. 264, 144–152.

Chang, Ch.Ch., Chiang, F.Ch., Chen, S.M., Thangavelu, K., Yang, H.J., 2016. Studies on electrochemical oxidation of aluminum and dyeing in various additives towards industrial applications. Int. J. Electrochem. Sci. 11, 2142–2152.

Chao, H.P., Wang, Y.C., Tran, H.N., 2018. Removal of hexavalent chromium from groundwater by Mg/Al-layered double hydroxides using characteristics of in-situ synthesis. Environ. Pollut. 243, 620–629.

Cheruiyot, G.K., Wanyonyi, W.C., Kiplimo, J.J., Maina, E.N., 2019. Adsorption of toxic crystal violet dye using coffee husks: equilibrium, kinetics and thermodynamics study. Sci. Afr. 5, e00116.
Chu, W., 2001. Dye removal from textile dye wastewater using recycled alum sludge. Water Res. 35, 3147–3152.
Coates, J., 2000. Interpretation of infrared spectra, a practical approach. In: Meyers, R.A. (Ed.), Encyclopedia of analytical chemistry. John Wiley & Sons Ltd., Chichester, UK.
Collivignarelli, M.C., Abbà, A., Miino, M.C., Damiani, S., 2019. Treatments for color removal from wastewater: state of the art. J. Environ. Manag. 236, 727–745.
Condi de Godoi, F., Rodriguez-Castellon, E., Guibal, E., Beppu, M.M., 2013. An XPS study of chromate and vanadate sorption mechanism by chitosan membrane containing copper nanoparticles. Chem. Eng. J. 234, 423–429.
Cornell, R.M., Schwertmann, U., 2003. The Iron Oxides: Structure, Properties, Reactions, Occurrences and Uses, 2nd, Completely Revised and, Extended Edition. Wiley-VCH, Weinheim.
Daud, M., Hai, A., Banat, F., Wazir, M.B., Habib, M., Bharath, G., Al-Harthi, M.A., 2019. A review on the recent advances, challenges and future aspect of layered double hydroxides (LDH) – containing hybrids as promising adsorbents for dyes removal. J. Mol. Liq. 288, 110989.
Deliz Quiñones, K., Hovsepyan, A., Oppong-Anane, A., Bonzongo, J.-C.J., 2016. Insights into the mechanisms of mercury sorption onto aluminum based drinking water treatment residuals. J. Hazard Mater. 307, 184–192.
Deng, S., Ting, Y.P., 2005. Fungal biomass with grafted poly(acrylic acid) for enhancement of Cu(II) and Cd(II) biosorption. Langmuir: ACS J. Surfaces Colloids. 21, 5940–5948.
Dias Monte Blanco, S.P., Scheufele, F.B., Módenes, A.N., Espinoza-Quiñones, F.R., Marin, P., Kroumov, A.D., Borba, C.E., 2017. Kinetic, equilibrium and thermodynamic phenomenological modeling of reactive dye adsorption onto polymeric adsorbent. Chem. Eng. J. 307, 466–475.
Eris, S., Azizian, S., 2017. Analysis of adsorption kinetics at solid/solution interface using a hyperbolic tangent model. J. Mol. Liq. 231, 523–527.
Foo, K.Y., Hameed, B.H., 2010. Insights into the modeling of adsorption isotherm systems. Chem. Eng. J. 156, 2–10.
Freundlich, H.M.F., 1906. Über die Adsorption in Lösungen (Over the adsorption in solution). Zeitschrift Für Physikalische Chemie (J. Phys. Chem.) 57, 385.
Furer, V.L., Vandyukov, A.E., Kleshnina, S.R., Solovieva, S.E., Antipin, I.S., Kovalenko, V.I., 2020. FT-IR and FT-Raman study of p-sulfonatocalix [8]arene. J. Mol. Struct. 1203, 127474.
Furlan, F.R., Melo da Silva, L.G., Morgado, A.F., Ulson de Souza, A.A., Ulson de Souza, S.M.A.G., 2010. Removal of reactive dyes from aqueous solutions using combined coagulation/flocculation and adsorption on activated carbon. Resour. Conserv. Recycl. 54, 283–290.
Gadekar, M.R., Ahammed, M.M., 2018. Modelling dye removal by adsorption onto water treatment residuals using combined response surface methodology-artificial neural network approach. J. Environ. Manag. 231, 241–248.
Grace Pavithra, K., Kumar, P.S., Jaikumar, V., Rajan, P.S., 2019. Removal of colorants from wastewater: a review on sources and treatment strategies. J. Ind. Eng. Chem. 75, 1–19.
Grosvenor, A.P., Kobe, B.A., Biesinger, M.C., McIntyre, N.S., 2004. Investigation of multiplet splitting of Fe 2p XPS spectra and bonding in iron compounds. Surf. Interface Anal. 36 (12), 1564–1574.
Gusain, R., Gupta, K., Joshi, P., Khatri, O.P., 2019. Adsorptive removal and photocatalytic degradation of organic pollutants using metal oxides and their composites: a comprehensive review. Adv. Colloid Interface Sci. 272, 102009.
Hadnadjev, M., Vulic, T., Marinkovic-Neducin, R., Suchorski, Y., Weiss, H., 2008. The iron oxidation state in Mg–Al–Fe mixed oxides derived from layered double hydroxides: an XPS study. Appl. Surf. Sci. 254 (14), 4297–4302.
Haerifar, M., Azizian, S., 2013. Mixed surface reaction and diffusion-controlled kinetic model forAdsorption at the solid/solution interface. J. Phys. Chem. C 117, 8310–8831.
Hedricks, D.W., 2006. Water Treatment Unit Processes: Physical and Chemical. CRC Press, Taylor & Francis Group, Boca Raton.
Ho, Y.S., McKay, G., 1999. Pseudo-second order model for sorption processes. Process Biochem. 34, 451–465.
Hossain, M.A., Ngo, H.H., Guo, W., 2013. Introductory of Microsoft Excel SOLVER function – spreadsheet method for isotherm and kinetics modelling of metals biosorption in water and wastewater. JWS 3, 223. http://waynehilldesign.com/images/brochures/RAP_capabilities.pdf%20.
Hubbe, M.A., Azizian, S., Douven, S., 2019. Implications of apparent pseudo-second-order adsorption kinetics onto cellulosic materials: a review. BioResources 14 (3), 7582–7626.
Jeppu, G.P., Clement, T.P., 2012. A modified Langmuir-Freundlich isotherm model for simulating pH-dependent adsorption effects. J. Contam. Hydrol. 129–130 (15), 46–53.
Kayranli, B., 2011. Adsorption of textile dyes onto iron based waterworks sludge from aqueous solution; isotherm, kinetic and thermodynamic study. Chem. Eng. J. 173, 782–791.
Kale, R.D., Kane, P.B., 2019. Colour removal of phthalocyanine based reactive dye by nanoparticles. Groundwater Sustain. Dev. 8, 309–318.
Kaludjerovic-Radoicica, T., Raicevic, S., 2010. Aqueous Pb sorption by synthetic and natural apatite: kinetics, equilibrium, and thermodynamic studies. Chem. Eng. J. 160 (2), 503.
Kang, D., Hu, C., Zhu, Q., 2018. Morphology controlled synthesis of hierarchical structured Fe_2O_3 from natural ilmenite and its high performance for dyes adsorption. Appl. Surf. Sci. 459, 327–335.
Khosravi, M., Azizian, S., 2014a. Adsorption of anionic dyes from aqueous solution by iron oxide nanospheres. J. Ind. Eng. Chem. 20, 2561–2567.
Khosravi, M., Azizian, S., 2014b. Synthesis of different nanostructured flower-like iron oxides and study of their performance as adsorbent. Adv. Powder Technol. 25, 1578–1584.
Kim, T.-H., Park, C., Shin, E.-B., Kim, S., 2004. Decolorization of disperse and reactive dye solutions using ferric chloride. Desalination 161, 49–58.
Koble, R.A., Corrigan, T.E., 1952. Adsorption isotherms for pure hydrocarbons. Ind. Eng. Chem. 44, 383–387.
Kumar, K.V., Gadipelli, S., Wood, B., Ramisetty, K.A., Stewart, A.A., Howard, C.A., Brett, D.J.L., Rodriguez-Reinoso, F., 2019. Characterization of the adsorption site energies and heterogeneous surfaces of porous materials. J. Mater. Chem. A. 7, 10104–10137.
Lagergren, S., 1898. About the theory of so-called adsorption of soluble substances. K. Sven. Vetensk. Handl. 24 (4), 1–39.
Langmuir, I., 1918. The adsorption of gases on plane surfaces of glass, mica and platinum. J. Am. Chem. Soc. 40, 1361.
Launer, P.J., 2013. Updated by Barry Arkles. infrared analysis of organosilicon compounds: spectra-structure correlations. Silicon compounds: silanes & silicones. In: Arkles, Barry, Larson, Gerald L. (Eds.), Infrared Analysis of Organosilicon Compounds, third ed. Gelest Inc., pp. 175–178 Chapter. https://www.researchgate.net/publication/272481071_Infrared_Analysis_of_Organosilicon_Compounds%20
Leiviskä, T., Leskelä, T., Tanskanen, J., 2019. Effect of alkali regeneration on pore characteristics and performance of ferric oxyhydroxide and akaganéite sorbents. J. Water Process Eng. 31, 100838.
Li, X.Q., Zeng, H.C., 2012. Calcium carbonate nanotablets: bridging artificial to natural nacre. Adv. Mater. 24, 6277–6282.
Lima, E.C., Hosseini-Bandegharaei, A., Moreno-Piraján, J.C., Anastopoulos, I., 2019. A critical review of the estimation of the thermodynamic parameters on adsorption equilibria. Wrong use of equilibrium constant in the Van't Hoof equation for calculation of thermodynamic parameters of adsorption. J. Mol. Liq. 273, 425–434.
Lv, S., Zhou, Z., Xue, M., Zhang, X., Yang, Z., 2020. Adsorption characteristics of reactive blue 81 by powdered activated carbon: role of the calcium content. J. Water Process Eng. 36, 101247.
Machado, F.M., Bergmann, C.P., Lima, E.C., Adebayo, M.A., Fagan, S.B., 2014. Adsorption of a textile dye from aqueous solutions by carbon nanotubes. Mat. Res. 17, 153–160.
Mahapatra, N.N., 2016. Textile Dyes. Woodhead Publishing India Pvt Ltd., New Delhi.
Mahmoud, H.R., El-Molla, S.A., Saif, M., 2013. Improvement of physicochemical properties of Fe_2O_3/MgO nanomaterials by hydrothermal treatment for dye removal from industrial wastewater. Powder Technol. 249, 225–233.
McIntyre, N.S., Zetaruk, G., 1977. X-ray photoelectron spectroscopic studies of iron oxides. Anal. Chem. 49 (11), 1521–1529.
McKay, G., Mesdaghinia, A., Nasseri, S., Hadi, M., Aminabad, M.S., 2014. Optimum isotherms of dyes sorption by activated carbon: fractional theoretical capacity & error analysis. Chem. Eng. J. 251 (1), 236–247.
Mikhaylov, V.I., Maslennikova, T.P., Ugolkov, V.L., Krivoshapkin, P.V., 2016. Hydrothermal synthesis, characterization and sorption properties of Al/Fe oxide–oxyhydroxide composite powders. Adv. Powder Technol. 27, 756–764.
Moghaddam, S.S., Alavi Moghaddam, M.R., Arami, M., 2010. A comparison study on acid red 119 dye removal using two different types of waterworks sludge. Water Sci. Technol. 61, 1673–1681.
Momina, Mohammad, S., Isamil, S., 2020. Study of the adsorption/desorption of MB dye solution using bentonite adsorbent coating. J. Water Process Eng. 34, 101155.
Najafpoor, A., Alidadi, H., Esmaeili, H., Hadilou, T., Dolatabadi, M., Hosseinzadeh, A., Davoudi, M., 2016. Optimization of anionic dye adsorption onto Melia azedarach sawdust in aqueous solutions: effect of calcium cations. Asia-Pacific Journal of Chemical Engineering Asia-Pac. J. Chem. Eng. 11, 258–270.
Nassar, N.N., 2010. Kinetics, mechanistic, equilibrium, and thermodynamic studines on the adsorption of acid red dye from wastewater by γ-Fe_2O_3 nanoadsorbents. Sep. Sci. Technol. 45, 1092–1103.
Navarro, A., Sanz, F., 1999. Dye aggregation in solution: study of C.I. direct red I. Dyes Pigments 40, 131–139.
Ni, M., Ratner, B.D., 2008. Differentiating calcium carbonate polymorphs by surface analysis techniques—an XPS and TOF-SIMS study. Surf. Interface Anal. 40 (10), 1356–1361.
Nourmoradi, H., Pourzamani, H., Zabihollahi, S., 2015. Removal of a common textile dye, navy blue (NB), from aqueous solutions by combined process of coagulation–flocculation followed by adsorption. Desalin. Water Treat. 57, 1–12.
Novoselova, L.Y., 2013. Composition, structure, and sorbability of the thermally treated water deironing precipitate with respect to carbon monoxide. Powder Technol. 243, 149–154.
Ociński, D., Jacukowicz-Sobala, I., Mazur, P., Raczyk, J., Kociołek-Balawejder, E., 2016. Water treatment residuals containing iron and manganese oxides for arsenic removal from water – characterization of physicochemical properties and adsorption studies. Chem. Eng. J. 294, 210–221.
Özacar, M., Şengil, I.A., 2005. A kinetic study of metal complex dye sorption onto pine sawdust. Process Biochem. 40 (2), 565–572.
Redlich, O., Peterson, D.L., 1959. A useful adsorption isotherm. J. Phys. Chem. 63, 1024.
Roginsky, S., Zeldovich, Y.B., 1934. The catalytic oxidation of carbon monoxide on manganese dioxide. Acta Phys. Chem. USSR 1, 554.
Sanodure Green LWN Safety Data Sheet, 2020. Clariant. https://www.clariant.com/en/Solutions/Products/2014/03/18/17/07/Sanodure-Green-LWN.
Senthil Kumar, P., Ramalingam, S., Senthamarai, C., Niranjanaa, M., Vijayalakshmi, P., Sivanesan, S., 2010. Adsorption of dye from aqueous solution by cashew nut shell: studies on equilibrium isotherm, kinetics and thermodynamics of interactions. Desalination 261, 52–60.

Shahwan, T., 2015. Lagergren equation: can maximum loading absorption replace equilibrium loading? Chem. Eng. Res. Des. 96, 172–176.
Sips, R., 1948. On the structure of a catalyst surface. J. Chem. Phys. 16, 490.
Su, D., Kim, H.-S., Kim, W.-S., Wan, G., 2012. Synthesis of tuneable porous hematites (α-Fe_2O_3) for gas sensing and lithium storage in lithium ion batteries. Microporous Mesoporous Mater. 149, 36–45.
Sutherland, C., Venkobachar, C., 2010. A diffusion-chemisorption kinetic model for simulating biosorption using forest macro-fungus, fomes fasciatus. Int. Res. J. Plant Sci. 1 (4), 107–117.
Szostak, K., Banach, M., 2019. Sorption and photocatalytic degradation of methylene blue on bentonite-ZnO-CuO nanocomposite. J. Mol. Liq. 286, 110859.
Tan, K.L., Hameed, B.H., 2017. Insight into the adsorption kinetics models for the removal of contaminants from aqueous solutions. J. Taiwan Inst. Chem. Eng. 74, 25–48.
Temkin, M.I., Pyzhev, V., 1940. Kinetics of ammonia synthesis on promoted iron catalyst. Acta Phys. Chim. USSR 12, 327–356.
Thommes, M., Kaneko, K., Neimark, A.V., Olivier, J.P., Rodriguez-Reinoso, F., Rouquerol, J., Sing, K.S.W., 2015. Physisorption of gases, with special reference to the evaluation of surface area and pore size distribution (IUPAC Technical Report). Pure Appl. Chem. 87, 1051–1069.
Toth, J., 1971. State equation of the solid gas interface layer. Acta Chem. Acad. Hung. 69, 311–317.
Tran, H.N., You, S.-J., Hosseini-Bandegharaei, A., Chao, H.P., 2017. Mistakes and inconsistencies regarding adsorption of contaminants from aqueous solutions: a critical review. Water Res. 120, 88.
Usman, F., Dennis, J.O., Seong, K.C., Ahmed, A.Y., Meriaudeau, F., Ayodele, O.B., Tobi, A.R., Rabih, A.A.S., Yar, A., 2019. Synthesis and characterisation of a ternary composite of polyaniline, reduced graphene-oxide and chitosan with reduced optical band gap and stable aqueous dispersibility. Results Phys. 15, 102690.
Vu, A.-T., Vu, V.-T., 2018. Preparation of MgO for removal of dyes and heavy metal from aqueous solution: facially controlling the morphology, kinetic, isotherms and thermal dynamic investigations. Indian J. Sci. Technol. 11.
Walker, G.M., Weatherley, L.R., 2001. Adsorption of dyes from aqueous solution—the effect of adsorbent pore size distribution and dye aggregation. Chem. Eng. J. 83, 201–206.
Wang, J., Guo, X., 2020. Adsorption isotherm models: classification, physical meaning, application and solving method. Chemosphere 258, 127279.
Wang, S., Li, H., 2007. Kinetic modelling and mechanism of dye adsorption on unburned carbon. Dyes Pigm. 72, 308–314.
Xie, S., Wen, Z., Zhan, H., Jin, M., 2018. An experimental study on the adsorption and desorption of Cu(II) in silty clay. Hindawi Geofluids. Article ID 3610921, 12.
Yildiz, E., Boztepe, H., 2002. Synthesis of novel acidic mono azo dyes and an investigation of their use in textile industry. Turk. J. Chem. 26, 897–903.
Yoon, T.H., Johnson, S.B., Brown, G.E., 2005. Adsorption of organic matter at mineral/water interfaces. IV. Adsorption of humic substances at boehmite/water interfaces and impact on boehmite dissolution. Lagmuir 21 (11), 5002–5012.
Zhang, Y.-X., Jia, Y., 2018. Fluoride adsorption on manganese carbonate: ion-exchange based on the surface carbonate-like groups and hydroxyl groups. J. Coll. Interface Sci. 510, 407–417.
Zhang, R., Leiviskä, T., Tanskanen, J., Gao, B., Yue, Q., 2019. Utilization of ferric groundwater treatment residuals for inorganic-organic hybrid biosorbent preparation and its use for vanadium removal. Chem. Eng. J. 361, 680–689.
Zhu, S., Fang, S., Huo, M., Yu, Y., Chen, Y., Yang, X., Geng, Z., Wang, Y., Bian, D., Huo, H., 2015. A novel conversion of the groundwater treatment sludge to magnetic particles for the adsorption of methylene blue. J. Hazard Mater. 292, 173–179.
Zubrytė, E., Gefenienė, A., Kauspėdienė, D., Ragauskas, R., Binkienė, R., Selskienė, A., Pakštas, V., 2019. Fast removal of Pb(II) and Cu(II) from contaminated water by groundwater treatment waste: impact of sorbent composition. Separ. Sci. Technol.